ESC Cardiovascular Research (2026) **122**, 412–426
https://doi.org/10.1093/cvr/cvag009

Semaphorin 7A aggravates abdominal aortic aneurysm through PDK1/SGK3/YTHDC1 axis-mediated phenotypic switching of vascular smooth muscle cells

Fengchan Li [1,2†], Zhen Zhu[1†], Fan Tang[1†], Yun Du[1], Jiaxin Lyu[1], Lili Wu[2], Haofu Ni[1], Ying Wang[1], Lijie Ren[1], Qiongyu Lu[1], Huihui Liu[3], Lei Hong[4], Hongjie Wang[5], Chaojun Tang[1,6,7,8*], and Li Zhu [2,6,7*]

[1]Cyrus Tang Medical Institute, Soochow University, Suzhou, China; [2]Department of Laboratory Medicine, Suzhou Ninth Hospital Affiliated to Soochow University, Suzhou, China; [3]Department of Neurology and Clinical Research Center of Neurological Disease, Second Affiliated Hospital, Soochow University, Suzhou, China; [4]Department of Vascular Surgery, The First Affiliated Hospital of USTC, Anhui, China; [5]Division of Cardiology, Department of Internal Medicine, Tongji Hospital, Huazhong University of Science and Technology, Wuhan, China; [6]Collaborative Innovation Center of Hematology of Jiangsu Province, Soochow University, Suzhou, China; [7]National Clinical Research Center for Hematologic Diseases, the First Affiliated Hospital of Soochow University, Suzhou, China; and [8]Department of Cardiology, The First People's Hospital of Taicang, Taicang Affiliated Hospital of Soochow University; Soochow University, Suzhou, China

Received 10 June 2025; revised 23 September 2025; accepted 26 October 2025; online publish-ahead-of-print 19 January 2026

Time of primary review: 35 days

See the editorial comment for this article 'SEMA7A-mediated regulation of smooth muscle cell plasticity in AAA: a potential intersection with metabolic reprogramming in the aortic wall', by D.F.J. Ketelhuth, https://doi.org/10.1093/cvr/cvag024.

Aims Semaphorin 7A (SEMA7A), a membrane-anchored glycoprotein involved in immune and vascular signalling, has been implicated in cardiovascular diseases. However, its role in the development of abdominal aortic aneurysm (AAA) has not been defined. In this study, we investigated the role of SEMA7A in AAA progression and the underlying mechanisms.

Methods and results A meta-analysis of genome-wide association studies identified SEMA7A as a candidate gene involved in AAA formation. Global and vascular smooth muscle cell (VSMC)-specific *Sema7a* knockout mice were generated and subjected to a $CaPO_4$-induced AAA model. Compared with wild-type controls, SEMA7A-deficient mice exhibited a 28.6% reduction in aortic expansion, a finding that was recapitulated in VSMC-specific *Sema7a* knockout mice. RNA sequencing of $CaPO_4$-stimulated mouse VSMCs, along with immunofluorescence staining of AAA tissues, revealed that SEMA7A deficiency suppressed VSMC phenotypic switching. Further mechanistic studies demonstrated that SEMA7A promotes this switching via the integrin α5β1-mediated PDK1/SGK3/YTHDC1 signalling axis. Notably, administration of a synthetic SEMA7A-mimicking small peptide, ACP, significantly inhibited VSMC phenotypic switching and attenuated AAA progression.

Conclusion This study underscores the critical role of SEMA7A in regulating VSMC phenotypic switching through a novel PDK1/SGK3/YTHDC1 axis, which contributes to AAA pathogenesis, suggesting that targeting SEMA7A is a promising therapeutic strategy for AAA prevention and treatment.

* Corresponding author. Li Zhu, Suzhou Ninth Hospital Affiliated to Soochow University, Suzhou, Jiangsu, China, E-mail: zhul@suda.edu.cn or Chaojun Tang, Cyrus Tang Medical Institute, Taicang Affiliated Hospital of Soochow University, Soochow University; Tel: 86-512-65880877-3509, Fax: 86-512-65882122. E-mail: zjtang@suda.edu.cn.
† These authors contributed equally.

Graphical Abstract

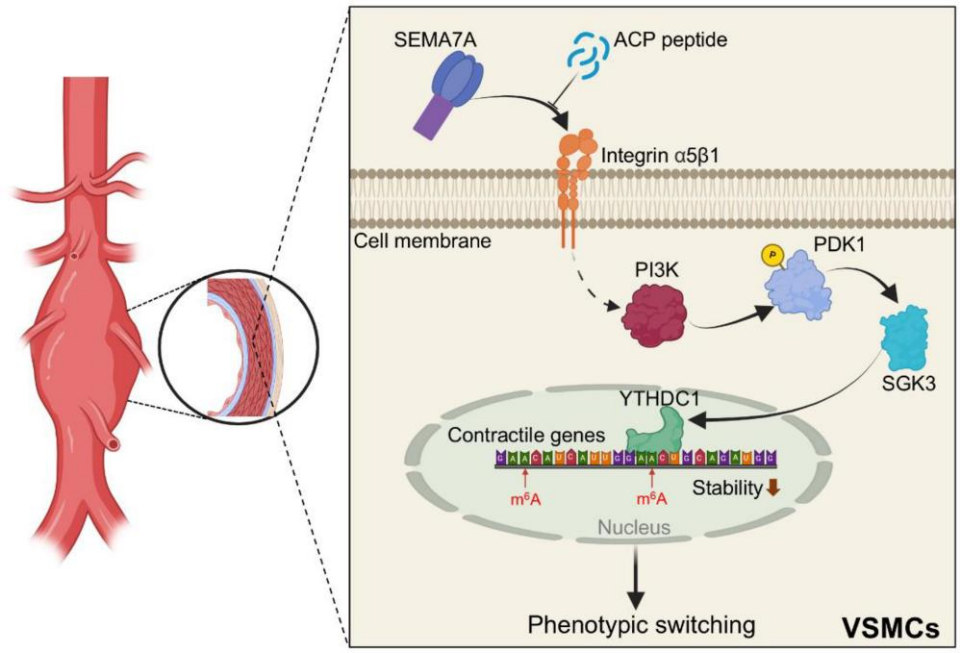

Keywords Abdominal aortic aneurysm SEMA7A • Phenotypic switching • Vascular smooth muscle cell • Peptide

1. Introduction

Abdominal aortic aneurysm (AAA) is a serious and potentially fatal condition characterized by permanent regional dilation of the abdominal aorta exceeding 1.5 times its normal diameter. This pathological enlargement can lead to aortic rupture and sudden death.[1] Although AAA often remains asymptomatic during its early stages, rupture is associated with a mortality rate exceeding 80%.[2] While surgical interventions such as open repair and endovascular aneurysm repair (EVAR) are currently the mainstays of treatment,[3] no effective pharmacological therapies exist to halt or reverse disease progression. Therefore, there is an urgent need to elucidate the molecular mechanisms driving AAA pathogenesis to identify novel therapeutic targets.

A key histopathological hallmark of AAA is medial degeneration, which compromises the structural integrity of the abdominal aorta and contributes to its dilation and potential rupture.[4] This degeneration is closely linked to the phenotypic switching of VSMCs within the tunica media. Under pathological stimuli, VSMCs undergo a transition from a contractile phenotype to a synthetic phenotype, a critical early event in AAA pathogenesis.[1,5] Dedifferentiated VSMCs not only contribute to extracellular matrix (ECM) degradation through the production of matrix metalloproteinases (MMPs),[6,7] but also intensify vascular inflammation by secreting proinflammatory cytokines.[8] Consequently, identifying and targeting key regulators of VSMC phenotypic switching offers a promising strategy for the AAA treatments.

Semaphorin 7A (SEMA7A) is a distinctive member of the class VII semaphorin subfamily, characterized by glycosylphosphatidylinositol (GPI)-anchored membrane association.[9] Although traditionally recognized for its role in axon guidance within the nervous system,[10] emerging evidence suggests that SEMA7A plays pivotal roles in a range of inflammation-related diseases, including cancer,[11–13] sepsis,[14,15] obesity,[16] multiple sclerosis,[17,18] and cardiovascular diseases.[19,20]

Our previous studies demonstrated that SEMA7A deficiency attenuates atherosclerotic plaque formation by reducing leukocyte adhesion induced by disturbed blood flow.[19] Endothelial SEMA7A has been implicated in endothelial-to-mesenchymal transition (EndMT) via TGF-β2/Smad signalling, mediated by the transcription factor ATF3.[21] Although the pathological mechanisms of atherosclerosis and AAA differ in several respects, they share many common pathogenic features, including vascular inflammation,[22] vascular calcification,[23] and phenotypic modulation of vascular cells.[6] Given this overlap, the present study aimed to elucidate the signalling pathways through which SEMA7A contributes to AAA development and to evaluate its potential as a therapeutic target.

2. Methods

2.1 Human samples

Human serum samples and AAA tissues were obtained from the First Affiliated Hospital of the University of Science and Technology of China (USTC). This study was approved by the Research Ethics Committee of the First Affiliated Hospital of USTC (Approval No: 2024-RE-467). This study was also conducted in accordance with the Declaration of Helsinki. All patients were fully informed about the research and provided written informed consent. The baseline characteristics of the enrolled patients with AAA and control subjects are provided in Supplementary material online, *Table S1*.

2.2 Animals

The animal protocol for this study was approved by the Ethics Committee of Soochow University (Approval No:

SUDA20250429A03). *Sema7a*-flox mice were generated by the CAM-SU Genomic Resource Center at Soochow University. Mouse strains, including the *Sema7a* knockout, *Myh11-CreER*^{T2}, *Cdh5-Cre*, and *LysM-Cre* strains, were obtained from Jackson Laboratory (Bar Harbor). To generate VSMC-specific *Sema7a*-knockout mice (*Sema7a*$^{\Delta SMC}$), *Sema7a*-flox mice were crossed with *Myh11-CreER*^{T2} mice. CreERT2 recombinase activation in *Sema7a*$^{\Delta SMC}$ mice was induced by administering tamoxifen (75 mg/kg body weight) via intraperitoneal injection every 24 h for five consecutive days. Endothelial cell (EC)-specific *Sema7a*-knockout mice (*Sema7a*$^{\Delta EC}$) were generated by crossing *Sema7a*-flox mice with *Cdh5-Cre* mice, whereas myeloid cell-specific *Sema7a*-knockout mice (*Sema7a*$^{\Delta M\phi}$) were generated by crossing *Sema7a*-flox mice with *LysM-Cre* mice. All mice used were on a C57BL/6J background, with at least six generations of backcrossing to ensure genetic consistency. All the animal experiments were conducted under specific pathogen-free barrier conditions and in compliance with the institutional guidelines of the Laboratory Animal Center of Soochow University. All procedures followed the guidelines from Directive 2010/63/EU of the European Parliament. The mice were anaesthetized with 240 mg/kg tribromoethanol via intraperitoneal injection in order to produce less bradycardia with less effect on cardiac loading and ventricular function than does xylazine–ketamine.[24] At the appropriate time, the mice were euthanized with CO_2.

2.3 Cell experiments with inhibitors

Mouse VSMCs were seeded into 6-well plates and allowed to adhere overnight. The cells were then pretreated with one of the following inhibitors for 12 h: SGK3-PROTAC1 (SGK3 INH, 3 μM, T13847, TargetMol), obtustatin (α1β1 INH, 5 μM, T78219, TargetMol), ATN-161 (α5β1 INH, 5 μM, T10397, TargetMol) or integrin-IN-1 (αvβ1 INH, 5 μM, T13473, TargetMol). After pretreatment, the cells were exposed to 0.05 M $CaPO_4$ for 30 min, followed by the addition of the same concentration of the respective inhibitor. The cells were then cultured for an additional 48 h.

2.4 Administration of synthetic peptides

The scrambled peptide and SEMA7A RGD-containing peptide (ACP) were synthesized by TGpeptide Biotechnology (Nanjing, China). The peptides were verified via high-performance liquid chromatography and mass spectrometry (MS) characterization. To evaluate the preventive effects of ACP, peptides (scrambled or ACP) were administered intravenously at a dose of 25 mg/kg one day before AAA model induction. The same dose was subsequently administered every three days for two weeks. To assess the therapeutic effects of ACP, peptides (scrambled or ACP) were administered intravenously at a dose of 50 mg/kg starting on day 7 after $CaPO_4$-induced AAA induction. For this therapeutic regimen, injections were given every two days.

2.5 Statistical analysis

Differentially expressed genes (DEGs) for RNA-seq analysis were identified via the Wald test, as implemented in the 'DESeq2' package. Statistical analyses were performed via Prism 8.0 (GraphPad Prism Software). An unpaired two-tailed Student's *t* test was used to evaluate differences between groups, with statistical significance defined as $P < 0.05$ (*), $P < 0.01$ (**), $P < 0.001$ (***), and $P < 0.0001$ (****). The data are presented as the mean ± SEM.

The detailed experimental protocols and materials used for this study are provided in the Methods section of the Supplementary Material.

3. Results

3.1 Increased SEMA7A expression is associated with AAA

To investigate the potential association between semaphorins and AAA, we screened single nucleotide polymorphisms (SNPs) in semaphorin-related genes using data from a genome-wide association study (GWAS) meta-analysis encompassing 39 221 individuals with AAA.[25] This analysis identified a significant association between the intronic variant rs11856835 at the SEMA7A locus and AAA, reaching the genome-wide significance threshold ($P < 5 \times 10^{-8}$) (*Figure 1A*, Supplementary material online, *Table S2*). This association has also been previously reported,[26] further substantiating the relevance of this variant in AAA pathogenesis. To assess the potential functional impact of rs11856835, we analysed cis-expression quantitative trait locus (cis-eQTL) data from the eQTLGen consortium and found a positive correlation between rs11856835 and SEMA7A expression (*Figure 1B*). Supporting this genetic evidence, analysis of human serum samples revealed significantly elevated SEMA7A levels in AAA patients compared with healthy adults (*Figure 1C*). Notably, immunofluorescence analysis revealed co-localization of SEMA7A with α-SMA$^+$ VSMCs in human AAA tissues (see Supplementary material online, *Figure S1A*).

To further investigate the biological implications of SEMA7A in AAA, we performed gene set enrichment analysis (GSEA) in VSMCs overexpressing SEMA7A (*Figure 1D*). GSEA revealed a significant enrichment of genes involved in cartilage development, a process implicated in vascular calcification.[27,28] Consistently, SEMA7A overexpression markedly upregulated the expression of vascular calcification-related genes (*Figure 1E*), including SPP1,[29] BMP4,[30] and BMP6.[31] Given the emerging role of vascular calcification as both a hallmark and potential driver of AAA progression,[23] we employed a calcium phosphate ($CaPO_4$)-induced AAA mouse model, which recapitulates key pathological features of human AAA, including elastin degradation and vascular calcification.[32,33]

Histological analysis via Von Kossa staining and protein quantification by Western blotting confirmed that robust calcification in $CaPO_4$-treated aortic tissues (*Figure 1F*), accompanied by elevated SEMA7A expression (*Figure 1G*). Additionally, immunofluorescence staining demonstrated spatial co-localization of SEMA7A with BMP4 (*Figure 1H*) and a marked increase in SEMA7A expression (*Figure 1I*), suggesting a potential mechanistic link between SEMA7A and calcification processes during AAA development. Taken together, these findings provide compelling evidence for a strong association between increased SEMA7A expression and AAA, implicating SEMA7A as a potential contributor to disease pathogenesis.

3.2 Global or VSMC-specific deletion of *Sema7a* mitigates AAA development

To elucidate the role of SEMA7A in AAA development, *Sema7a*$^{+/+}$ and *Sema7a*$^{-/-}$ mice were subjected to $CaPO_4$ application to the abdominal aorta. As shown in *Figure 2A*, SEMA7A deficiency attenuated aneurysm formation. The mean abdominal aorta diameter in *Sema7a*$^{-/-}$ mice was 28.6% smaller compared to *Sema7a*$^{+/+}$ mice ($P < 0.01$) (*Figure 2B* and *C*). Further histological assessments via haematoxylin and eosin (H&E) staining and Victoria blue (VB) staining revealed that SEMA7A deficiency mitigated vascular lesions and elastin degradation (*Figure 2D* and *E*), suggesting a protective role of SEMA7A deficiency against $CaPO_4$-induced AAA.

Although elevated SEMA7A expression was observed both in AAA patient serum and in $CaPO_4$-induced AAA mouse models, the cellular source and mechanistic contribution of SEMA7A remain unclear. To clarify this, we performed immunofluorescent

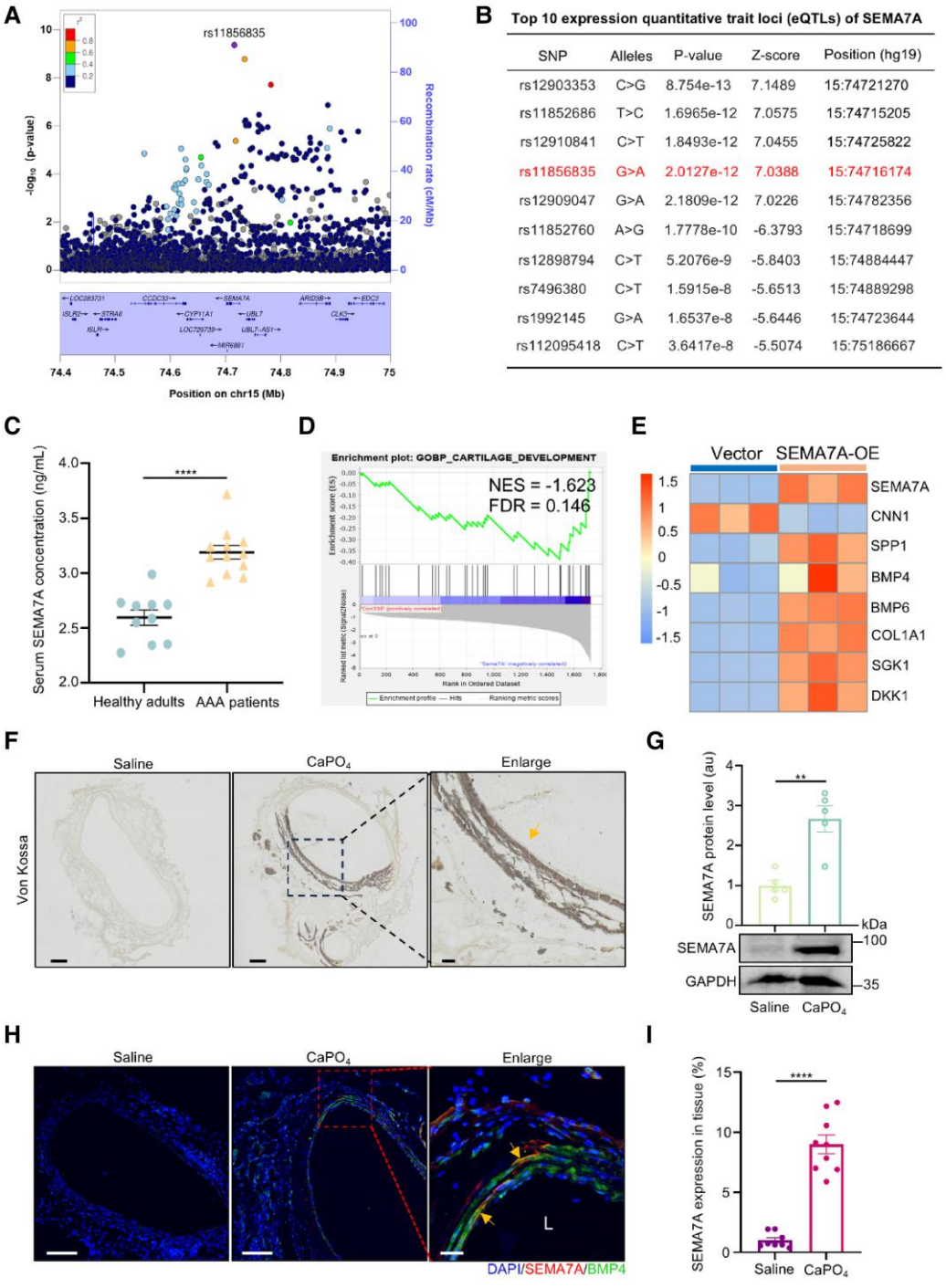

Figure 1 Increased SEMA7A expression is associated with AAA. (*A*) Identification of the AAA-associated single-nucleotide polymorphism (SNP) rs11856835 at the SEMA7A locus via meta-analysis of the AAAgen consortium. (*B*) The top 10 significant genetic variants significantly associated with SEMA7A expression were identified via cis-expression quantitative trait locus (cis-eQTL) analysis from the eQTLGen Consortium. (*C*) Serum SEMA7A levels in AAA patients vs. healthy adults. Data are presented as mean ± SEM, ****$P < 0.0001$, Student's *t*-test. (*D*) Gene set enrichment analysis (GSEA) based on the Gene Ontology (GO) biological process database revealed that the cartilage development pathway was enriched in SEMA7A-overexpressing HA-VSMCs. (*E*) Heatmap showing the expression levels of the contractile marker CNN1 and calcification-related molecules in human VSMCs overexpressing SEMA7A. (*F*) Von Kossa staining demonstrated vascular calcification in $CaPO_4$-induced AAA tissues in mice. Scale bars = 100 μm (left and middle) or 20 μm (right). (*G*) Western blot analysis of SEMA7A protein levels in $CaPO_4$-induced AAA tissues. Data are presented as mean ± SEM, **$P < 0.01$, Student's *t*-test. $n = 5$ mice per group. au: arbitrary units. (*H*) Immunofluorescence staining of SEMA7A and BMP4 in $CaPO_4$-induced mouse AAA tissues and (*I*) statistical analyses of SEMA7A expression in AAA tissues. Data are presented as mean ± SEM, ****$P < 0.0001$, Student's *t*-test. SEMA7A, red; BMP4, green; DAPI, blue. Scale bars = 100 μm (left and middle) or 20 μm (right).

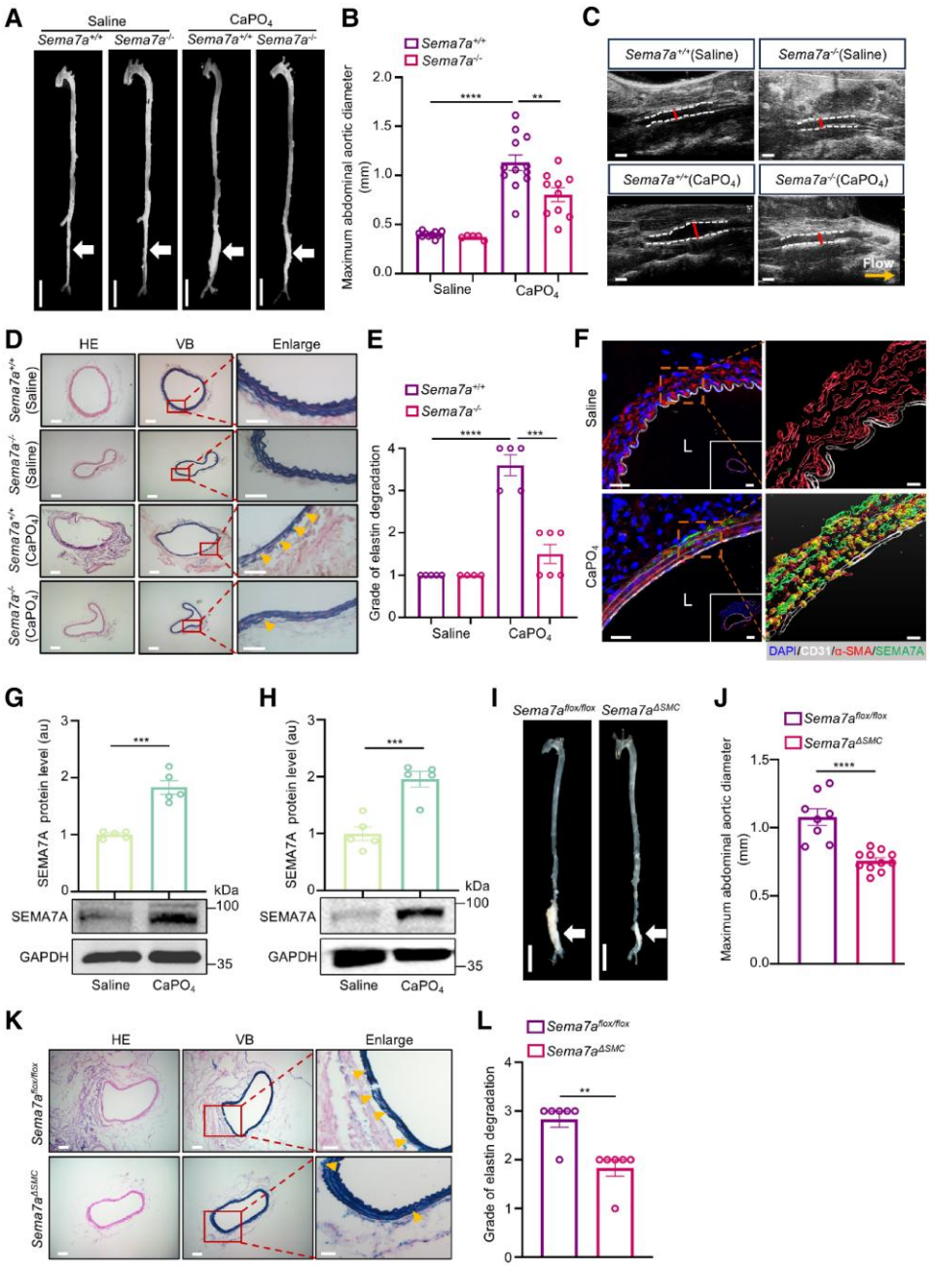

Figure 2 Global or VSMC-specific deletion of *Sema7a* mitigates AAA development. (*A*) Representative microscopy images of the abdominal aorta. Scale bars = 2 mm. (*B*) Quantification of the maximal aortic diameter via *ImageJ* software. The data are presented as mean ± SEM, $^{**}P < 0.01$, $^{****}P < 0.0001$, Student's *t*-test, $n \geq 5$ mice per group. (*C*) Ultrasound images of abdominal aortas from *Sema7a*$^{+/+}$ and *Sema7a*$^{-/-}$ mice at 2 weeks post-$CaPO_4$ stimulation. Scale bars = 1 mm. (*D*) Representative images of H&E and Victoria blue (VB) staining of abdominal aortas from *Sema7a*$^{+/+}$ and *Sema7a*$^{-/-}$ mice. Scale bars = 50 μm (left and middle) or 20 μm (right). (*E*) Quantification of elastin degradation in each group. The data are presented as mean ± SEM, $^{***}P < 0.001$, $^{****}P < 0.0001$, Student's *t*-test. (*F*) Representative images of immunofluorescence staining (left) and 3D reconstruction (right) of the aorta following $CaPO_4$ treatment. SEMA7A, green; CD31, white; α-SMA, red; DAPI, blue. Scale bars = 20 μm (left), 200 μm (middle) or 5 μm (right). (*G*, *H*) Western blot analysis of the SEMA7A protein in $CaPO_4$-stimulated primary mouse VSMCs (*G*) or in human aortic vascular smooth muscle cells (HA-VSMCs) following $CaPO_4$ stimulation (*H*). Representative immunoblots are shown, and the results are presented as mean ± SEM, $^{***}P < 0.001$, Student's *t*-test. *n* (the number of biological replicates) = 5 in each group. au: arbitrary units. (*I*) Representative images of abdominal aortas from *Sema7a*$^{\Delta SMC}$ and *Sema7a*$^{flox/flox}$ mice in the $CaPO_4$-induced AAA model. Scale bars = 2 mm. (*J*) Quantification of the maximal aortic diameter in each group via *ImageJ* software. The data are presented as mean ± SEM, $^{****}P < 0.0001$, Student's *t*-test, $n \geq 8$ mice per group. (*K*) H&E and VB staining of $CaPO_4$-induced AAA tissues. Scale bars = 50 μm (left and middle) or 20 μm (right). (*L*) Quantification of elastin degradation in *Sema7a*$^{\Delta SMC}$ and *Sema7a*$^{flox/flox}$ mice. The data are presented as mean ± SEM, $^{**}P < 0.01$, Student's *t*-test, $n = 6$ mice per group.

co-staining of lesioned aortic tissue using anti-SEMA7A antibody alongside antibodies of markers for macrophages, endothelial cells (ECs) and VSMCs. This analysis revealed a pronounced increase in SEMA7A levels specifically in VSMCs but not in ECs or macrophages (*Figure 2F*, Supplementary material online, *Figure S1B*). Supporting this finding, Western blot analysis demonstrated upregulated SEMA7A protein levels in mouse and human aortic VSMCs following $CaPO_4$ stimulation (*Figure 2G* and *H*).

To directly assess the cell type-specific contribution of SEMA7A, we generated conditional *Sema7a*-knockout mice targeting VSMCs ($Sema7a^{\Delta SMC}$), ECs ($Sema7a^{\Delta EC}$), and myeloid cells ($Sema7a^{\Delta M\phi}$) (see Supplementary material online, *Figure S2A-2C*), with $Sema7a^{flox/flox}$ used as controls. VSMC-specific deletion of *Sema7a* significantly ameliorated $CaPO_4$-induced AAA development (*Figure 2I* and *J*) and led to a reduction in vascular lesions, elastin fragmentation, and vascular inflammation (*Figure 2K* and *2L*, Supplementary material online, *Figure S3*). In contrast, deletion of *Sema7a* in ECs (see Supplementary material online, *Figure S4A-4E*) or myeloid cells (see Supplementary material online, *Figure S5A-5E*) did not affect AAA progression. Collectively, these findings establish that VSMC-derived SEMA7A plays a central role in AAA pathogenesis.

3.3 SEMA7A deficiency inhibits VSMC phenotypic switching in AAA

To elucidate the mechanism by which VSMC-derived SEMA7A contributes to $CaPO_4$-induced AAA, we performed RNA sequencing on VSMCs isolated from $Sema7a^{+/+}$ and $Sema7a^{-/-}$ mice following $CaPO_4$ stimulation. A total of 341 differentially expressed genes (DEGs) were identified, including 119 upregulated genes and 222 downregulated genes in $Sema7a^{-/-}$ VSMCs compared with wild-type controls (*Figure 3A*). Notably, genes associated with the synthetic phenotype of VSMCs, such as *Spp1*, *Ccl8*, *Nrp1*, and *Mmp13*, were significantly downregulated, while contractile phenotype markers, including *Cnn1*, *Ccn3*, *Acta1*, and *Actg2*, were markedly upregulated in $Sema7a^{-/-}$ VSMCs (*Figure 3B*). These transcriptomic findings were further validated using qRT–PCR (*Figure 3C*) and Western blot analysis, which confirmed a decrease in osteopontin (OPN, encoded by *Spp1*) and a concurrent increase in Calponin1 (encoded by *Cnn1*) in $Sema7a^{-/-}$ VSMCs (*Figure 3D*). In contrast, overexpression of SEMA7A in human aortic VSMCs induced VSMC phenotypic switching, characterized by reduced Calponin1 expression and increased OPN expression (*Figure 3E*). Moreover, SEMA7A overexpression significantly enhanced VSMC proliferation (see Supplementary material online, *Figure S6A*) and migration (see Supplementary material online, *Figure S6B*).

To determine whether these effects were preserved in vivo, we analysed markers of phenotypic switching in $CaPO_4$-induced AAA model using immunofluorescence staining (*Figure 3F*). In $Sema7a^{-/-}$ mice, OPN expression was significantly reduced (*Figure 3G*), whereas Calponin1 expression was markedly increased (*Figure 3H*), resulting in a lower OPN/Calponin1 ratio (*Figure 3I*). Taken together, these findings identify SEMA7A as a novel driver of VSMC phenotypic modulation, thereby contributing to AAA pathogenesis in $CaPO_4$-induced model.

3.4 SEMA7A promotes VSMC phenotypic switching via the PDK1/SGK3/YTHDC1 signalling pathway

To elucidate the molecular mechanism by which SEMA7A promotes VSMC phenotypic switching, we performed Kyoto Encyclopedia of Genes and Genomes (KEGG) pathway analysis on DEGs between $Sema7a^{+/+}$ and $Sema7a^{-/-}$ VSMCs. The top five enriched signalling pathways included cell adhesion molecules, the PI3K–Akt signalling pathway, malaria, viral protein interactions with cytokines, and cytokine receptors and cytokine–cytokine receptor interactions (*Figure 4A*). Notably, the PI3K–Akt pathway presented the greatest proportion of DEGs, prompting us to further investigate its role in SEMA7A-driven VSMC phenotypic switching.

Western blot analysis revealed that although PI3 K and AKT phosphorylation remained unchanged, PDK1 phosphorylation was significantly decreased in $Sema7a^{-/-}$ VSMCs following $CaPO_4$ stimulation (*Figure 4B* and *C*). Since PDK1 activates both AKT-dependent and AKT-independent downstream targets, we examined its AKT-independent effector, serum/glucocorticoid-regulated kinase 3 (SGK3). The RNA sequencing data identified Sgk3 as one of the top four downregulated genes in the PI3K–Akt pathway in $Sema7a^{-/-}$ VSMCs (see Supplementary material online, *Figure S7*), a finding validated by Western blot (*Figure 4D*). To assess the functional relevance of SGK3, we treated primary VSMCs with SGK3-PROTAC1,[34] a selective SGK3 degrader, following $CaPO_4$ stimulation. Both Western blot and qRT–PCR analyses demonstrated that SGK3 inhibition significantly suppressed $CaPO_4$-induced VSMC phenotypic switching (*Figure 4E* and *F*). Conversely, SGK3 overexpression (SGK3-OE) induced VSMC phenotypic switching, even in the absence of $CaPO_4$ stimulation (*Figure 4G* and *H*). These results establish the PDK1/SGK3 axis as a crucial mediator of SEMA7A-induced VSMC phenotypic modulation.

To further delineate the downstream effectors of SGK3, we conducted nuclear proteomics analysis of VSMCs treated with SGK3-PROTAC1. A total of 339 differentially expressed nuclear proteins were identified, including YTH domain-containing protein 1 (YTHDC1) as the most significantly downregulated (*Figure 5A* and *B*). Western blot further confirmed reduced YTHDC1 expression following SGK3-PROTAC1 treatment (*Figure 5C*). To assess the role of YTHDC1, we generated shRNA-mediated *Ythdc1*-knockdown VSMCs and found that its depletion suppressed synthetic markers while enhancing contractile markers expression under $CaPO_4$ stimulation (*Figure 5D* and *E*), indicating that YTHDC1 promotes VSMC phenotypic switching. Moreover, SGK3 overexpression in SEMA7A-deficient mouse VSMCs restored YTHDC1 levels and promoted phenotypic switching (*Figure 5F*), confirming that SEMA7A regulates VSMC phenotypic switching through the PDK1/SGK3/YTHDC1 axis.

As a known m^6A reader, YTHDC1 modulates mRNA stability by binding methylated transcripts.[35,36] To explore whether this mechanism underlies its regulation of contractile genes, we used the SRAMP prediction tool to analyse m^6A modification sites in *Cnn1*, *Cnn3*, and *Acta1* transcripts. The results indicated that these contractile marker transcripts contained multiple m^6A sites (*Figure 5G-5I*). Treatment with actinomycin D, an RNA polymerase II inhibitor, demonstrated that *Ythdc1* knockdown significantly enhanced mRNA stability of these contractile markers (*Figure 5J-5L*), suggesting that YTHDC1 facilitates their mRNA degradation in an m^6A-dependent manner. Taken together, these findings establish that SEMA7A promotes VSMC phenotypic switching through activation of the PDK1/SGK3/YTHDC1 signalling axis, in part by the m^6A-dependent degradation of contractile markers mRNAs. This pathway provides a mechanistic link between SEMA7A signalling and VSMC dysfunction in AAA pathogenesis.

3.5 Interaction of SEMA7A with integrin α5β1 promotes VSMC phenotypic switching

SEME7A has been reported to activate downstream signalling pathways primarily through integrin β1,[9] PlexinC1,[37] or GPIb.[20] To determine whether these receptors mediate SEMA7A-induced VSMC phenotypic switching, we first examined the expression of integrin β1 (encoded by *Itgb1*) and PlexinC1 (encoded by *Plxnc1*), considering that GPIb has been identified as a SEMA7A receptor only in platelets.[20] RT–PCR analysis revealed the expression of *Itgb1* but not *Plxnc1* in both human and mouse VSMCs (*Figure 6A*). Consistently, Western blot analysis confirmed the absence of PlexinC1 expression even after $CaPO_4$ stimulation

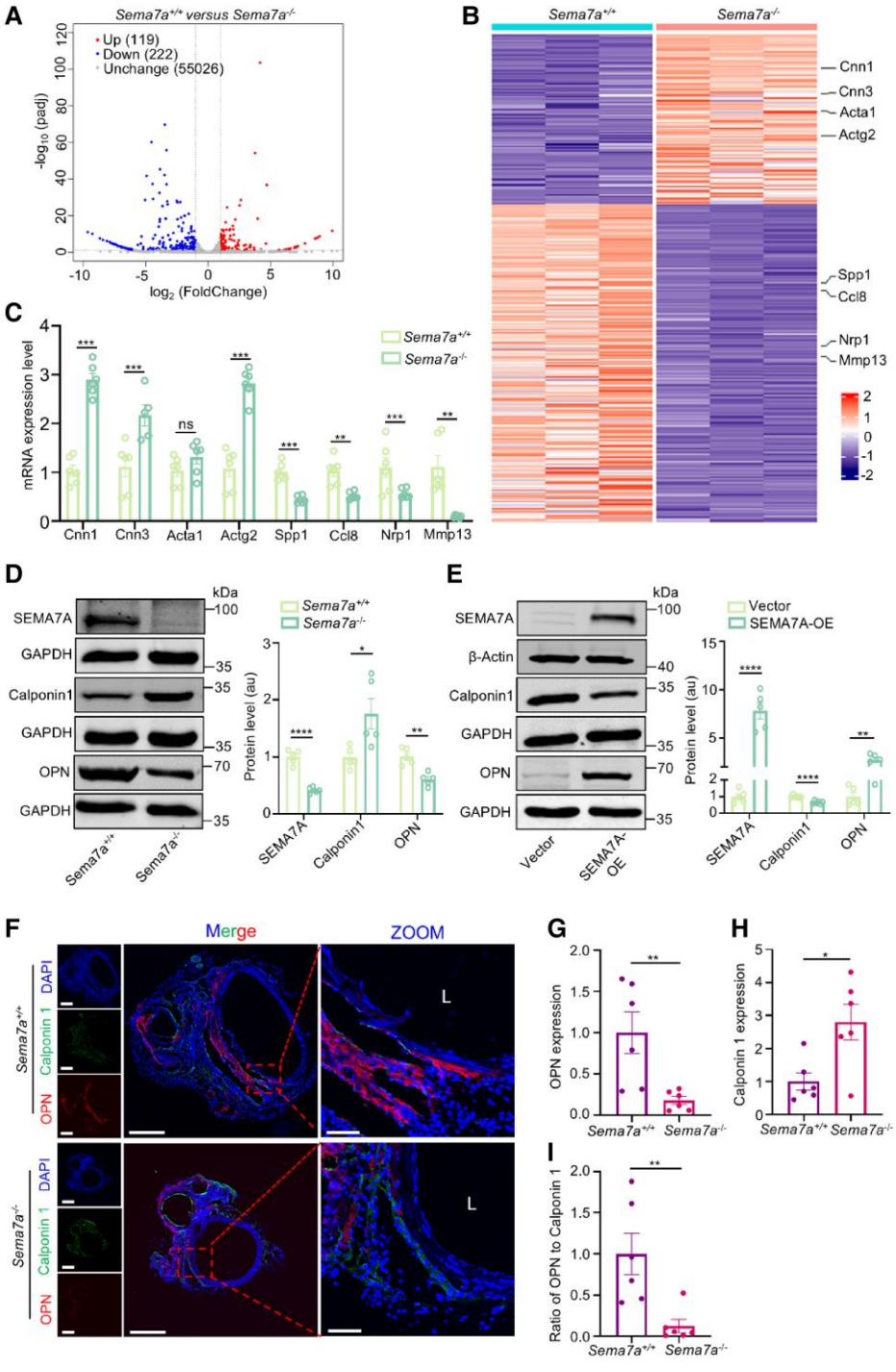

Figure 3 SEMA7A deficiency inhibits VSMC phenotypic switching in $CaPO_4$-induced AAA mouse model. (*A*) Volcano plot displaying the DEGs of VSMCs isolated from *Sema7a*$^{+/+}$ and *Sema7a*$^{-/-}$ mice after $CaPO_4$ stimulation. The DEGs of RNA-seq were analysed with Wald test. (*B*) Heatmap showing the expression levels of contractile and synthetic VSMC markers among the identified DEGs. (*C*) qRT–PCR analysis of contractile and synthetic VSMC marker gene expression shown in (*B*). Data are presented as mean ± SEM, $^{**}P < 0.01$, $^{***}P < 0.001$, Student's *t*-test. ns: not significant. (*D*) Western blot analysis showing the protein levels of SEMA7A, Calponin1 and OPN in VSMCs from *Sema7a*$^{+/+}$ and *Sema7a*$^{-/-}$ mice after $CaPO_4$ stimulation. The data are shown as mean ± SEM, $^{*}P < 0.05$, $^{**}P < 0.01$, $^{****}P < 0.0001$, Student's *t*-test. *n* (the number of biological replicates) = 5 in each group. (*E*) Western blot analysis of SEMA7A, Calponin1 and OPN protein levels in *Sema7a*-overexpressing (SEMA7A-OE) human aortic vascular smooth muscle cells (HA-VSMCs). The data are presented as mean ± SEM, $^{**}P < 0.01$, $^{****}P < 0.0001$, Student's *t*-test. *n* (the number of biological replicates) = 5 in each group. (*F–I*) Representative images (*F*) and statistical analyses (*G–I*) of the immunofluorescence staining of AAA tissues from *Sema7a*$^{+/+}$ and *Sema7a*$^{-/-}$ mice. OPN, red; Calponin1, green; DAPI, blue. Scale bars = 200 μm (left and middle) or 50 μm (right). The data are presented as mean ± SEM, $^{*}P < 0.05$, $^{**}P < 0.01$, Student's *t*-test, $n \geq 5$ mice per group.

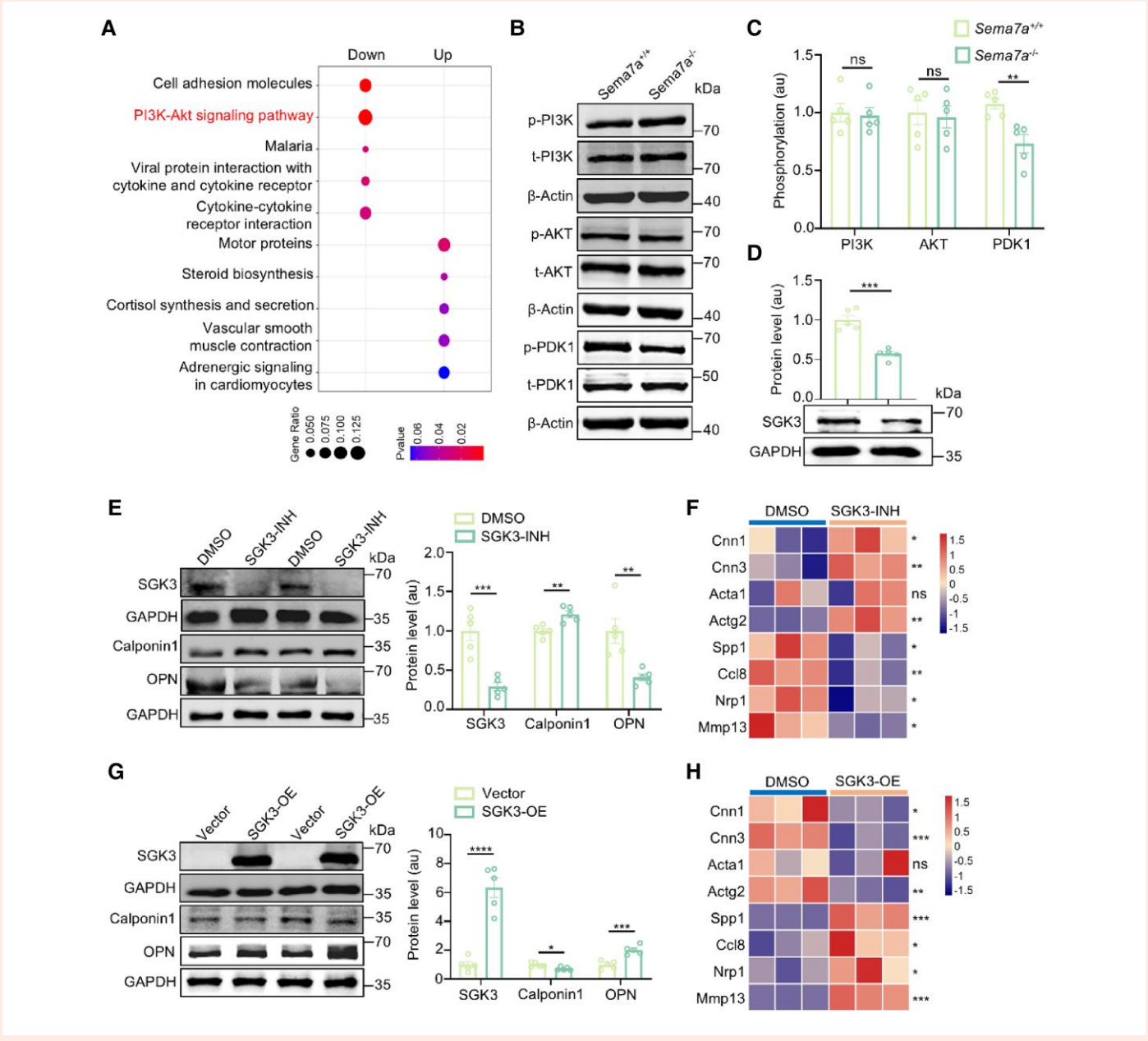

Figure 4 SEMA7A deficiency inhibits the PDK1/SGK3 pathway. (*A*) Bubble plot depicting the top 5 enriched Kyoto Encyclopedia of Genes and Genomes (KEGG) pathways in the upregulated or downregulated genes. (*B*, *C*) Western blot analysis of phosphorylated and total PI3 K (p-PI3 K, t-PI3 K), AKT (p-AKT, t-AKT) and PDK1 (p-PDK1, t-PDK1) protein levels in VSMCs from *Sema7a*$^{+/+}$ and *Sema7a*$^{-/-}$ mice after $CaPO_4$ stimulation. The results are presented as mean ± SEM, $^{**}P < 0.01$, Student's *t*-test. ns: not significant. *n* (the number of biological replicates) = 5 in each group. au: arbitrary units. (*D*) Western blot showing SGK3 protein levels in VSMCs from *Sema7a*$^{+/+}$ and *Sema7a*$^{-/-}$ mice after $CaPO_4$ stimulation. The results are presented as mean ± SEM, $^{***}P < 0.001$, Student's *t*-test. *n* (the number of biological replicates) = 5 in each group. au: arbitrary units. (*E*) Western blot showing SGK3, Calponin1 and OPN protein levels in $CaPO_4$-stimulated mouse VSMCs treated with SGK3-PROTAC1 (SGK3-INH). The results are presented as mean ± SEM, $^{**}P < 0.01$, $^{***}P < 0.001$, Student's *t*-test. *n* (the number of biological replicates) = 5 in each group. au: arbitrary units. (*F*) qRT–PCR analysis of contractile and synthetic marker gene expression in $CaPO_4$-stimulated VSMCs treated with SGK3-INH or DMSO. $^{*}P < 0.05$, $^{**}P < 0.01$, Student's *t*-test. (*G*) Western blot analysis of SGK3, Calponin1 and OPN protein levels in *Sgk3*-overexpressing (SGK3-OE) mouse primary VSMCs. The results are presented as mean ± SEM, $^{*}P < 0.05$, $^{***}P < 0.001$, $^{****}P < 0.0001$, Student's *t*-test. *n* (the number of biological replicates) = 5 in each group. au: arbitrary units. (*H*) Heatmap displaying the expression of contractile and synthetic VSMC markers in *Sgk3*-overexpressing mouse primary VSMCs. $^{*}P < 0.05$, $^{**}P < 0.01$, $^{***}P < 0.001$, Student's *t*-test.

(*Figure 6B*). Interestingly, while SEMA7A expression was upregulated following $CaPO_4$ stimulation, integrin β1 levels remained unchanged (*Figure 6B* and *C*). To assess whether integrin β1 directly interacts with SEMA7A in $CaPO_4$-stimulated VSMCs, co-immunoprecipitation assays were performed, revealing an interaction between endogenous integrin β1 and SEMA7A (*Figure 6D*).

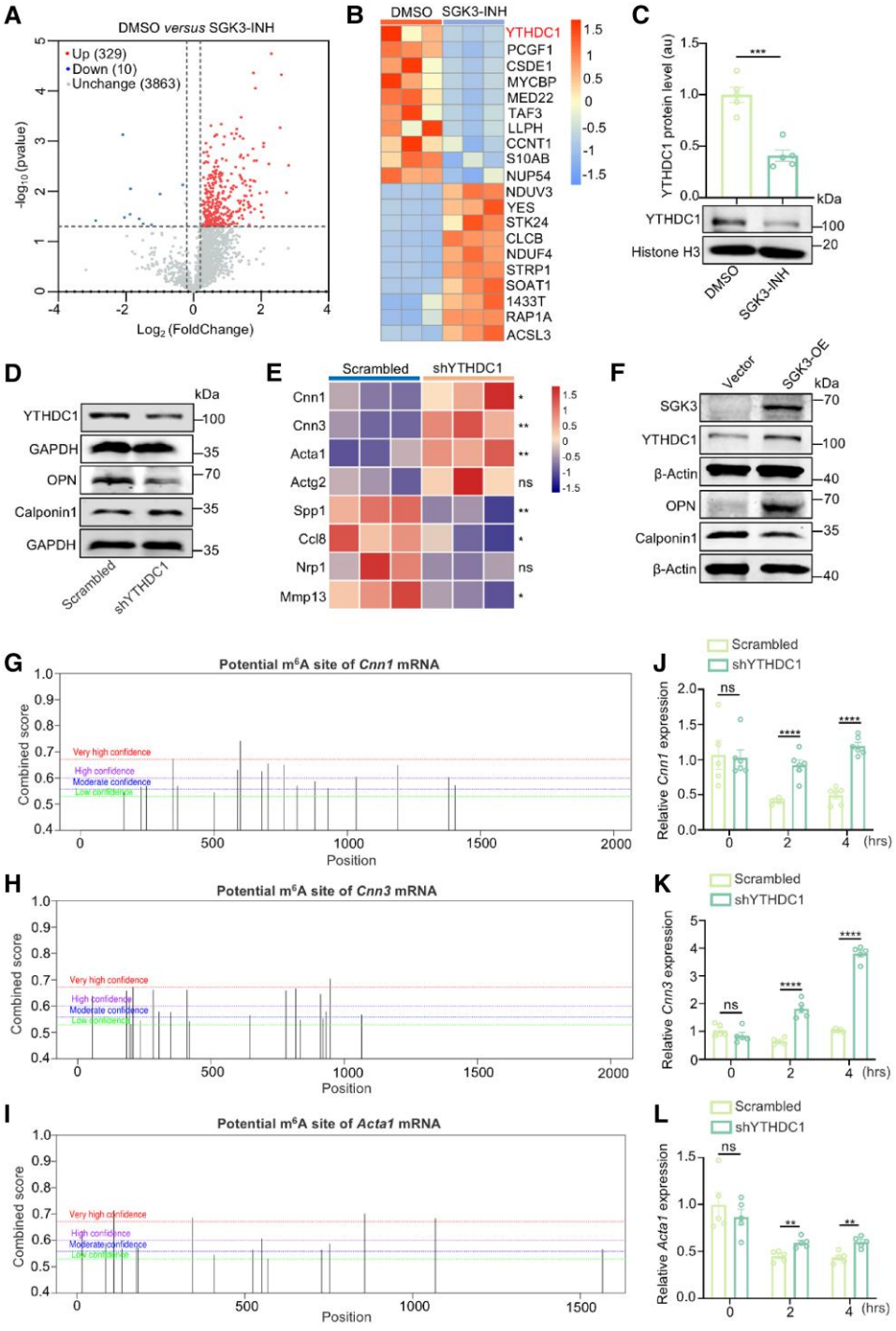

Figure 5 The m6a reader YTHDC1 is essential for SGK3-mediated VSMC phenotypic switching. (*A*) Volcano plot showing differentially expressed proteins in the DMSO- or SGK3-INH-treated groups. The differentially expressed proteins were analysed with Student's *t*-test. (*B*) Heatmap representing the relative expression levels of the top 10 differentially expressed proteins in the DMSO- or SGK3-INH-treated groups. (*C*) Western blot analysis of YTHDC1 protein levels in the nuclei of mouse VSMCs in the DMSO- or SGK3-INH-treated groups. The results are presented as mean ± SEM, ***$P < 0.001$, Student's *t*-test. *n* (the number of biological replicates) = 5 in each group. au: arbitrary units. (*D*) Western blot analysis of YTHDC1, OPN and Calponin1 expression in mouse VSMCs after shRNA-mediated *Ythdc1* knockdown. (*E*) qRT–PCR analysis of contractile and synthetic VSMC marker gene expression after *Ythdc1* knockdown under $CaPO_4$ stimulation. *$P < 0.05$, **$P < 0.01$, Student's *t*-test. (*F*) Western blot analysis of SGK3, YTHDC1, Calponin1, and OPN protein levels in SEMA7A-deficient mouse VSMCs following SGK3 overexpression (SGK3-OE). (*G–I*) m^6A sites were identified in the *Cnn1* (*G*), *Cnn3* (*H*) and *Acta1* (*I*) mRNAs via the SRAMP prediction server. (*J–L*) RNA stability of *Cnn1* (*J*), *Cnn3* (*K*) and *Acta1* (*L*) mRNAs measured by qRT–PCR after blocking new RNA synthesis with actinomycin D. Data are presented as mean ± SEM, **$P < 0.01$, ****$P < 0.0001$, Student's *t*-test. *n* (the number of biological replicates) ≥ 5 in each group. ns: not significant.

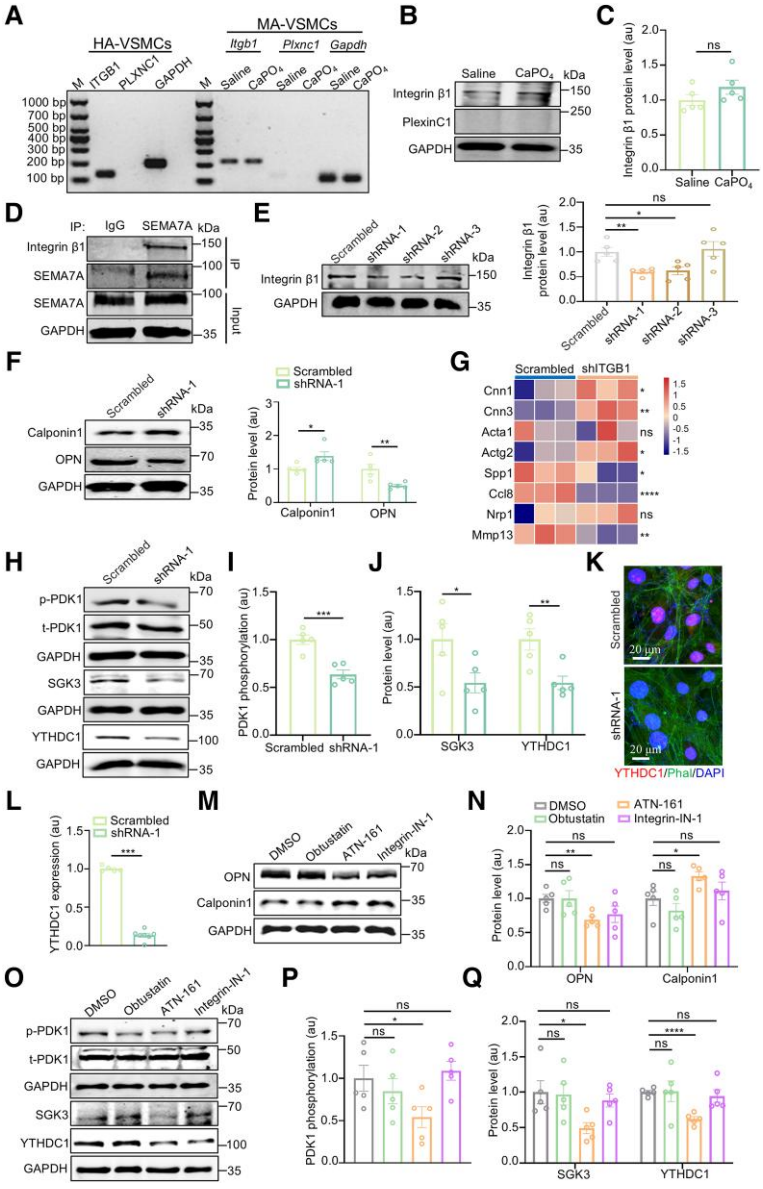

Figure 6 The interaction of SEMA7A with integrin α5β1 promotes VSMC phenotypic switching. (*A*) The mRNA levels of ITGB1 and PLXNC1 were examined by RT–PCR in HA-VSMCs and MA-VSMCs. (*B*, *C*) The protein levels of integrin β1 and PlexinC1 in mouse VSMCs treated with $CaPO_4$ or saline. The results of are presented as mean ± SEM, Student's *t*-test. *n* (the number of biological replicates) = 5 in each group. ns: not significant. au: arbitrary units. (*D*) Coimmunoprecipitation (co-IP) assay showing the interaction between integrin β1 and SEMA7A in $CaPO_4$-stimulated mouse primary VSMCs. The results are representative of 5 independent biological replicates. (*E*) The protein levels of integrin β1 in *Itgb1*-knockdown mouse VSMCs. The data are presented as mean ± SEM, $^*P < 0.05$, $^{**}P < 0.01$, Student's *t*-test. *n* (the number of biological replicates) = 5 in each group. (*F*) Calponin1 and OPN protein levels in *Itgb1*-knockdown mouse VSMCs treated with $CaPO_4$. The results are presented as mean ± SEM, $^*P < 0.05$, $^{**}P < 0.01$, Student's *t*-test. *n* (the number of biological replicates) = 5 in each group. au: arbitrary units. (*G*) mRNA levels of contractile and synthetic VSMC marker genes in *Itgb1*-knockdown mouse VSMCs after $CaPO_4$ stimulation. $^*P < 0.05$, $^{**}P < 0.01$, $^{****}P < 0.0001$, Student's *t*-test. ns: not significant. (*H*–*J*) Phosphorylation of PDK1 and protein levels of SGK3 and YTHDC1 in *Itgb1*-knockdown mouse VSMCs treated with $CaPO_4$. The results are presented as mean ± SEM, $^*P < 0.05$, $^{**}P < 0.01$, $^{***}P < 0.001$, Student's *t*-test. *n* (the number of biological replicates) = 5 in each group. au: arbitrary units. (*K*, *L*) Representative immunofluorescence images and statistical analyses of YTHDC1 in *Itgb1*-knockdown VSMCs after $CaPO_4$ stimulation. Phal: phalloidin. YTHDC1, red; Phal, green; DAPI, blue. Scale bars = 20 μm. The results are presented as mean ± SEM, $^{***}P < 0.001$, Student's *t*-test. *n* (the number of biological replicates) ≥ 5 in each group. (*M*, *N*) Protein levels of OPN and Calponin1 in $CaPO_4$-stimulated mouse VSMCs treated with obtustatin (an α1β1 inhibitor), ATN-161 (an α5β1 inhibitor) or integrin-IN-1 (an αvβ1 inhibitor). The data are presented as mean ± SEM, $^*P < 0.05$, $^{**}P < 0.01$, Student's *t*-test. *n* (the number of biological replicates) = 5 in each group. ns: not significant. au: arbitrary units. (O–Q) Phosphorylation of PDK1 and protein levels of SGK3 and YTHDC1 in $CaPO_4$-stimulated mouse VSMCs treated with inhibitors. The data are presented as mean ± SEM, $^*P < 0.05$, $^{****}P < 0.0001$, Student's *t*-test. *n* (the number of biological replicates) = 5 in each group. ns: not significant. au: arbitrary units.

To further evaluate the functional role of integrin β1, we used short hairpin RNA (shRNA) to knock down *Itgb1* expression in mouse VSMCs with three independent shRNAs (*Figure 6E*). Among them, shRNA-1 achieved the most efficient knockdown and was used in subsequent experiments. Western blotting and qRT–PCR analyses showed that *Itgb1* knockdown significantly reduced the expression of synthetic markers while increasing the expression of contractile markers in VSMCs (*Figure 6F* and *G*). These results suggest that integrin β1 mediates SEMA7A-induced phenotypic switching in $CaPO_4$-stimulated VSMCs. Further analysis revealed that *Itgb1* knockdown suppressed PDK1 phosphorylation (*Figure 6H* and *I*) and decreased SGK3 expression (*Figure 6H* and *J*), mimicking the signalling alterations observed in *Sema7a*-deficient cells. Additionally, both Western blotting (*Figure 6H* and *J*) and immunofluorescence staining (*Figure 6 K* and *6L*) demonstrated a significant reduction in YTHDC1 expression, indicating that integrin β1 is required for SEMA7A-mediated activation of the PDK1/SGK3/YTHDC1 axis.

Since ITGA1,[19] ITGA5,[38] and ITGAV,[39] as ITGB1-binding subunits, have been shown to mediate SEMA7A-induced cellular signalling, we next assessed their expression in primary mouse VSMCs using RT–PCR. *Itga1*, *Itga5*, and *Itgav* were all expressed in VSMCs even in the absence of $CaPO_4$ stimulation (see Supplementary material online, *Figure S8*). To identify the specific integrin β1-binding subunits involved in SEMA7A-induced phenotypic switching, VSMCs were pretreated with obtustatin (an α1β1 inhibitor), ATN-161 (an α5β1 inhibitor) or integrin-IN-1 (an αvβ1 inhibitor), followed by $CaPO_4$ stimulation for 48 h and Western blot analysis. The results revealed that integrin α5β1 was the predominant receptor mediating SEMA7A-induced phenotypic switching, in contrast to integrins α1β1 and αVβ1 (*Figure 6* M and 6N). Inhibition of integrin α5β1 also suppressed PDK1 phosphorylation (*Figure 6O* and *6P*) and reduced the expression of SGK3 and YTHDC1 (*Figure 6O* and *6Q*), consistent with the effects observed in *Itgb1*-knockdown cells. Collectively, these findings indicate that SEMA7A promotes VSMC phenotypic switching primarily through integrin α5β1-mediated activation of the PDK1/SGK3/YTHDC1 signalling pathway, thereby contributing to AAA pathogenesis.

3.6 Administration of an inhibitory peptide of SEMA7A retards the development of $CaPO_4$-induced AAA in mice

Given that the RGD (Arg-Gly-Asp) motif within the Sema domain of SEMA7A is recognized by integrin,[9] we hypothesize that a synthetic SEMA7A RGD-containing peptide could competitively inhibit the binding of SEMA7A to integrin β1, thereby preventing AAA development. To test this hypothesis, we designed a chimeric peptide consisting of the RGD sequence conjugated to the cell-penetrating peptide CGKRK, denoted as ACP (*Figure 7A*). To assess the stability and tissue retention of ACP in vivo, we synthesized rhodamine B-labelled ACP and administered it via tail vein injection in the $CaPO_4$-induced AAA model. Confocal imaging of AAA tissues collected at 1, 24, and 48 h post-injection revealed persistent rhodamine B fluorescence at all time points, whereas no signal was observed in vehicle-injected controls (see Supplementary material online, *Figure S9A*), indicating that ACP effectively accumulated and remained in the aneurysmal tissue for at least 48 h. In parallel, plasma analysis showed that more than 50% of the injected ACP remained in circulation at 48 h than at the 1-hour level (see Supplementary material online, *Figure S9B*), suggesting sustained systemic availability.

Encouraged by these findings, we next investigated the preventive potential of ACP in vivo. *Wild-type* mice received intravenous injections of ACP or a scrambled control peptide (25 mg/kg) one day before $CaPO_4$-induced AAA induction (*Figure 7B*). Stereomicroscope imaging revealed significantly reduced aneurysm formation in the ACP-treated group (*Figure 7C*). Quantitative assessment of maximal aortic diameter and vascular ultrasound imaging confirmed that ACP administration reduced $CaPO_4$-induced aortic dilation by 22.9% compared to the scrambled control (*Figure 7D* and *E*). Histological analyses, including H&E staining and Victoria blue staining, demonstrated that ACP treatment preserved vascular wall integrity and mitigated elastin degradation caused by $CaPO_4$ (*Figure 7F* and *G*). To evaluate whether ACP administration influences VSMC phenotypic switching *in vivo*, we performed immunofluorescence staining for VSMC markers (*Figure 7H*). ACP significantly increased the expression of the contractile marker Calponin1 (*Figure 7I*) and decreased the expression of the synthetic marker OPN in the tunica media (*Figure 7J*), resulting in a lower OPN/Calponin1 ratio compared with the scrambled peptide (*Figure 7 K*). Consistently, Western blot confirmed that ACP reduced OPN expression while increasing Calponin1 expression (*Figure 7L*). To further assess ACP's functional effects, a collagen gel contraction assay was conducted using human aortic VSMCs. ACP significantly enhanced the contractile capacity (*Figure 7 M*), suggesting its efficacy in preventing VSMC phenotypic switching *in vitro*.

To evaluate the therapeutic effects of ACP, peptides were intravenously administered at 50 mg/kg beginning on day 7 after $CaPO_4$-induced AAA induction, with injections repeated every two days. Maximal aortic diameter measurements showed that delayed ACP treatment reduced $CaPO_4$-induced aortic dilation by 26.7% compared to scrambled controls (*Figure 7N* and *7O*). Histological assessments further revealed improved vascular architecture and reduced elastin degradation in ACP-treated mice (*Figure 7P* and *7Q*). These findings indicate that ACP may serve as a promising therapeutic strategy for AAA treatment.

4. Discussion

This study identified SEMA7A as a critical contributor to the pathogenesis of AAA. A GWAS meta-analysis pinpointed an AAA-associated variant (rs11856835) within the SEMA7A locus. Elevated expression of SEMA7A was observed in both human AAA tissues and a murine $CaPO_4$-induced AAA model. Notably, global or VSMC-specific deletion of *Sema7a* significantly attenuated AAA progression in mice. Transcriptomic analyses of $CaPO_4$-stimulated VSMCs, alongside immunofluorescence staining of AAA tissue, revealed that SEMA7A deficiency suppresses VSMC phenotypic switching—a hallmark of aneurysm pathology. Mechanistically, SEMA7A promotes VSMC phenotypic switching primarily through integrin α5β1-mediated activation of the PDK1/SGK3/YTHDC1 signalling axis. Importantly, systemic administration of the synthetic SEMA7A peptide ACP inhibited VSMC phenotypic switching and halted AAA progression in mice, suggesting a promising preventive and therapeutic strategy for AAA.

SEMA7A has been implicated in various cardiovascular conditions, including atherosclerosis,[19] myocardial ischaemia,[20] viral myocarditis[40] and Kawasaki disease.[41] However, its role in AAA pathogenesis has remained largely unexplored. While Tang et al. reported elevated SEMA7A levels in AAA tissues, their study focused on SEMA4D and did not investigate the specific molecular mechanisms of SEMA7A in aneurysm development.[42] Our findings address this gap by demonstrating that *Sema7a* deletion in VSMCs protects against $CaPO_4$-induced AAA by inhibiting phenotypic switching via integrin α5β1. Although multiple receptors for SEMA7A have been reported, including integrin β1, PlexinC1, and GPIb, our data indicate that integrin β1 is the primary functional receptor in VSMCs, as PlexinC1 expression was negligible. We showed that *Itgb1* knockdown inhibited $CaPO_4$-induced VSMC phenotypic switching, which is consistent with previous findings that ITGB1 acts as a mediator of the

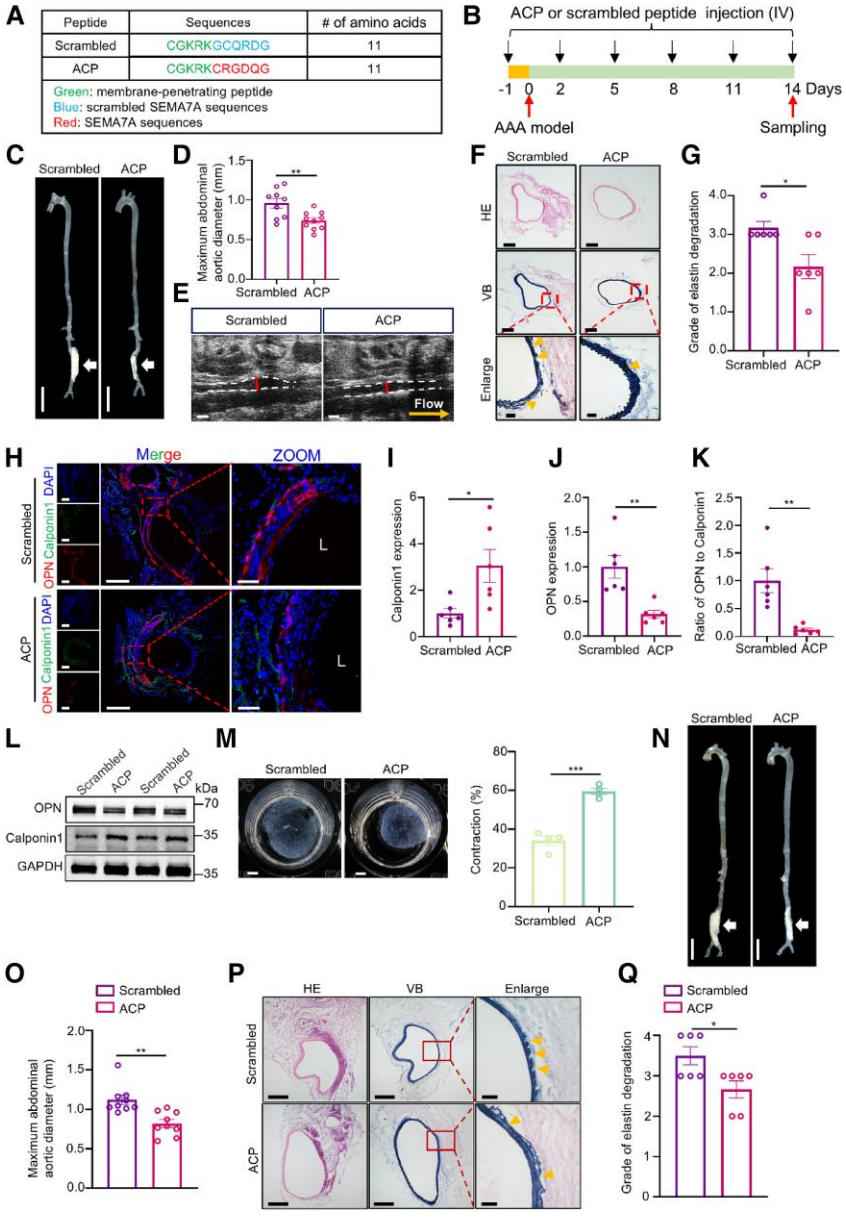

Figure 7 Administration of ACP mitigates the development of $CaPO_4$-induced AAA in mice. (*A*) Sequences of the ACP and scrambled peptide used in the study. (*B*) Experimental design for evaluating the effects of ACP administration in the $CaPO_4$-induced AAA model. (*C*) Representative macroscopic images of abdominal aortas from mice treated with ACP or scrambled peptides following $CaPO_4$-induced AAA. Scale bars = 2 mm. (*D*) Quantification of the maximal diameter of the abdominal aorta via *ImageJ* software. The data are presented as mean ± SEM, $^{**}P < 0.01$, Student's *t*-test, $n = 9$ or 10 mice per group. (*E*) Ultrasound imaging of abdominal aortas from mice treated with ACP or scrambled peptide at 2 weeks after $CaPO_4$ stimulation. Scale bars = 1 mm. (*F*) H&E and VB staining of $CaPO_4$-induced AAA tissues treated with ACP or scrambled peptides. Scale bars = 100 μm (top and middle) or 20 μm (bottom). (*G*) Quantification of elastin degradation in each group. The data are presented as mean ± SEM, $^{*}P < 0.05$, Student's *t*-test, $n = 6$ mice per group. (*H*–*K*) Immunofluorescence staining showing the expression of VSMC markers in AAA tissues from mice treated with ACP or the scrambled peptide. OPN, red; Calponin1, green; DAPI, blue. Scale bars = 200 μm (left and middle) or 50 μm (right). The data are presented as mean ± SEM, $^{*}P < 0.05$, $^{**}P < 0.01$, Student's *t*-test, $n \geq 5$ mice per group. (*L*) Protein levels of Calponin1 and OPN in $CaPO_4$-stimulated mouse VSMCs treated with 50 μM ACP or scrambled peptide. (*M*) ACP treatment restores contractility of human aortic VSMCs after CaPO4 stimulation in collagen gel contraction assay. The data are presented as mean ± SEM, $^{***}P < 0.001$, Student's *t*-test, $n = 4$ per group. Scale bars = 1 mm. (*N*) Representative macroscopic images of abdominal aortas from mice treated with 50 mg/kg scrambled peptide or ACP, starting on day 7 after $CaPO_4$-induced AAA induction. Injections were administered every two days. Scale bars = 2 mm. (*O*) Quantification of maximal abdominal aortic diameters in scrambled and ACP groups using *ImageJ* software. The data are presented as mean ± SEM, $^{**}P < 0.01$, Student's *t*-test, $n = 9$ mice per group. (*P*) Representative H&E and VB images of abdominal aortas from scrambled and ACP-treated groups. Scale bars = 100 μm (left and middle) or 20 μm (right). (*Q*) Quantification of elastin degradation in the scrambled and ACP groups. The data are presented as mean ± SEM, $^{*}P < 0.05$, Student's *t*-test, $n = 6$ mice per group.

effect of miR-134-5p on human VSMC phenotypic switching.[43] Our data further identify integrin α5β1 as the dominant heterodimer mediating SEMA7A-induced VSMC phenotypic switching, providing a clearer mechanistic basis for receptor specificity.

Unexpectedly, integrated transcriptomic and proteomic analyses revealed that SEMA7A signals through a PDK1/SGK3/YTHDC1 pathway. SGK3, a downstream effector of PDK1, is structurally related to AKT but functions in a distinct PI3K-dependent, AKT-independent axis.[44] Although integrin β1 has previously been implicated upstream of PI3 K/AKT signalling,[45–47] how it regulates SGK3 remains unclear and warrants further investigation. Additionally, YTHDC1, a m^6A RNA-binding protein, appears to regulate VSMC contractile gene expression via m^6A-mediated RNA decay. This finding aligns with previous work demonstrating that low-dose colchicine reduces AAA formation by inhibiting YTHDC1-mediated m^6A modification,[48] providing converging evidence for the importance of this pathway.

Interestingly, while SEMA7A plays a critical role in $CaPO_4$-induced AAA, we did not observe a similar effect on elastase-induced AAA (see Supplementary material online, Figure S10A-10E). This inconsistent observation may be due to the differences in the pathological processes involving SEMA7A in these two infrarenal AAA models. Unlike calcium phosphate-induced AAA, which not only induces VSMC phenotypic switching but also leads to vascular calcification,[32] elastase-induced AAA results primarily from the degradation of vascular elastin and the promotion of VSMC apoptosis.[49] Our immunofluorescence staining results also revealed differences in SEMA7A expression, as elastase treatment did not upregulate SEMA7A expression as $CaPO_4$ stimulation did (see Supplementary material online, *Figure S10F*). While both models are widely used for mechanistic studies of AAA and share features such as localized inflammation and extracellular matrix remodelling, they incompletely mimic the complexity of human AAA. Future studies should explore SEMA7A's role in the angiotensin II-induced suprarenal AAA model, which better reflects the systemic and haemodynamic components of human disease.

In this study, thoracic aortic VSMCs were used *in vitro*, suggesting that SEMA7A may also regulate phenotypic switching in VSMCs beyond the abdominal aorta. This raises the intriguing possibility that SEMA7A could play a broader role in thoracic aortic diseases such as thoracic aortic aneurysm (TAA) or dissection, warranting further investigation. Additionally, while elevated serum SEMA7A levels were observed in AAA patients, this increase is not necessarily unique to AAA, as SEMA7A is also upregulated in other inflammatory and vascular conditions, including acute atherothrombotic stroke.[50] These findings suggest that circulating SEMA7A may reflect a general inflammatory milieu rather than serve as a disease-specific marker. Therefore, its clinical diagnostic utility may depend on combination with other biomarkers to improve specificity. Moreover, systemic administration of ACP likely leads to its distribution across multiple organs, raising concerns about its off-target effects. Future studies should focus on developing targeted delivery systems to enhance cell-type specificity and reduce systemic exposure.

In conclusion, our study identified SEMA7A as a pivotal mediator of AAA through its interaction with integrin α5β1 and subsequent activation of the PDK1/SGK3/YTHDC1 signalling cascade, which promotes VSMC phenotypic switching. Importantly, administration of the synthetic peptide ACP effectively halted AAA progression, demonstrating its potential as a therapeutic strategy. These findings provide new mechanistic insights into AAA pathogenesis and highlight SEMA7A as a promising therapeutic target for AAA prevention and treatment.

Translational perspective

This study identifies SEMA7A as a key regulator of abdominal aortic aneurysm (AAA) through integrin α5β1-mediated PDK1/SGK3/YTHDC1 signalling, which drives vascular smooth muscle cell (VSMC) phenotypic switching. These findings enhance our understanding of AAA pathogenesis. Importantly, treatment with a synthetic SEMA7A small peptide (ACP) halted AAA progression, highlighting a promising therapeutic strategy for the prevention and treatment of AAA.

Supplementary material

Supplementary Methods; Supplementary Figure legends; Supplementary material online, *Figures S1–S10*; Supplementary material online, *Tables S1*, S2 and S3. Supplementary material is available at Cardiovascular Research online.

Authors' contributions

F.L., Z.Z., C.T., and L.Z. designed the research. F.L., Z.Z., F.T., Y.D., J.L., L.W., H.N., Y.W., L.R., and Q.L. performed the experiments and analysed the data. H.L., L.H., and H.W. provided the reagents or materials and participated in the experimental design. F.L., C.T., and L.Z. drafted and revised the manuscript.

Conflict of interest: The authors declare that no competing interests exist.

Funding

This work was supported by grants from the Natural Science Foundation of China (82170466, 82470483 to L.Z., 82070450 to C.T., 82200142 to L.R.), the Natural Science Foundation of Jiangsu Province (BK20230487 to F.L.), the fellowship of China Postdoctoral Science Foundation (7121102223 to F.L.), the Interdisciplinary Basic Frontier Innovation Program of Suzhou Medical College of Soochow University (YXY2304066 to Q.L.), the Suzhou Science and Technology Development Project (SKY2022109 to Q.L.) and the Priority Academic Program Development of Jiangsu Higher Education Institutions of China (to L.Z.).

Data availability

The RNA sequencing data have been deposited in publicly accessible repositories under accession number PRJNA1189864. The mass spectrometry proteomics data are available through the ProteomeXchange Consortium via the PRIDE partner repository with the dataset identifier PXD058108. Additional data that support the findings of this study are available from the corresponding authors upon reasonable request.

References

1. Wen Y, Liu Y, Li Q, Tan J, Fu X, Liang Y, Tuo Y, Liu L, Zhou X, LiuFu D, Fan X, Chen C, Chen Z, Wang Z, Fan S, Liu R, Pan L, Zhang Y, Tang WH. Spatiotemporal ATF3

expression determines VSMC fate in abdominal aortic aneurysm. *Circ Res* 2024;**134**:1495–1511.
2. Guo X, Zhong J, Zhao Y, Fu Y, Sun LY, Yuan A, Liu J, Chen AF, Pu J. LXRalpha promotes abdominal aortic aneurysm formation through UHRF1 epigenetic modification of miR-26b-3p. *Circulation* 2024;**150**:30–46.
3. Rokosh RS, Starnes BW, Chaikof EL. Society for vascular surgery implementation of clinical practice guidelines for patients with an abdominal aortic aneurysm: repair of an abdominal aortic aneurysm. *J Vasc Surg* 2021;**73**:1485–1487.
4. Le S, Wu J, Liu H, Du Y, Wang D, Luo J, Yang P, Ran S, Hu P, Chen M, Ye P, Xia J. Single-cell RNA sequencing identifies interferon-inducible monocytes/macrophages as a cellular target for mitigating the progression of abdominal aortic aneurysm and rupture risk. *Cardiovasc Res* 2024;**120**:1351–1364.
5. Gurung R, Choong AM, Woo CC, Foo R, Sorokin V. Genetic and epigenetic mechanisms underlying vascular smooth muscle cell phenotypic modulation in abdominal aortic aneurysm. *Int J Mol Sci* 2020;**21**:6334.
6. Petsophonsakul P, Furmanik M, Forsythe R, Dweck M, Schurink GW, Natour E, Reutelingsperger C, Jacobs M, Mees B, Schurgers L. Role of vascular smooth muscle cell phenotypic switching and calcification in aortic aneurysm formation. *Arterioscler Thromb Vasc Biol* 2019;**39**:1351–1368.
7. Song T, Zhao S, Luo S, Chen C, Liu X, Wu X, Sun Z, Cao J, Wang Z, Wang Y, Yu B, Zhang Z, Du X, Li X, Han Z, Chen H, Chen F, Wang L, Wang H, Sun K, Han Y, Xie L, Ji Y. SLC44A2 regulates vascular smooth muscle cell phenotypic switching and aortic aneurysm. *J Clin Invest* 2024;**134**:e173690.
8. Du LJ, Sun JY, Zhang WC, Liu Y, Liu Y, Lin WZ, Liu T, Zhu H, Wang YL, Shao S, Zhou LJ, Chen BY, Lu H, Li RG, Jia F, Duan SZ. NCOR1 maintains the homeostasis of vascular smooth muscle cells and protects against aortic aneurysm. *Cell Death Differ* 2023;**30**:618–631.
9. Pasterkamp RJ, Peschon JJ, Spriggs MK, Kolodkin AL. Semaphorin 7A promotes axon outgrowth through integrins and MAPKs. *Nature* 2003;**424**:398–405.
10. Inoue N, Nishizumi H, Naritsuka H, Kiyonari H, Sakano H. Sema7A/PlxnCl signaling triggers activity-dependent olfactory synapse formation. *Nat Commun* 2018;**9**:1842.
11. Liu Z, Meng X, Zhang Y, Sun J, Tang X, Zhang Z, Liu L, He Y. FUT8-mediated aberrant N-glycosylation of SEMA7A promotes head and neck squamous cell carcinoma progression. *Int J Oral Sci* 2024;**16**:26.
12. Garcia-Areas R, Libreros S, Simoes M, Castro-Silva C, Gazaniga N, Amat S, Jaczewska J, Keating P, Schilling K, Brito M, Wojcikiewicz EP, Iragavarpu-Charyulu V. Suppression of tumor-derived Semaphorin 7A and genetic ablation of host-derived Semaphorin 7A impairs tumor progression in a murine model of advanced breast carcinoma. *Int J Oncol* 2017;**51**:1395–1404.
13. Tarullo SE, Hill RC, Hansen KC, Behbod F, Borges VF, Nelson AC, Lyons TR. Postpartum breast cancer progression is driven by semaphorin 7a-mediated invasion and survival. *Oncogene* 2020;**39**:2772–2785.
14. Korner A, Bernard A, Fitzgerald JC, Alarcon-Barrera JC, Kostidis S, Kaussen T, Giera M, Mirakaj V. Sema7A is crucial for resolution of severe inflammation. *Proc Natl Acad Sci U S A* 2021;**118**:e2017527118.
15. Granja T, Kohler D, Tang L, Burkard P, Eggstein C, Hemmen K, Heinze KG, Heck-Swain KL, Koeppen M, Gunther S, Blaha M, Magunia H, Bamberg M, Konrad F, Ngamsri KC, Fuhr A, Keller M, Bernard AM, Haeberle HA, Bakchoul T, Zarbock A, Nieswandt B, Rosenberger P. Semaphorin 7A coordinates neutrophil response during pulmonary inflammation and sepsis. *Blood Adv* 2024;**8**:2660–2674.
16. Lu Q, Liu Z, Zhao L, Xu L, Liu C, Li L, Cao Y, Li F, Wu L, Wang L, Chen T, You T, Ren L, Wang G, Tang C, Zhu L. Sema7A protects against high-fat diet-induced obesity and hepatic steatosis by regulating adipo/lipogenesis. *Mol Metab* 2023;**70**:101698.
17. Eixarch H, Gutierrez-Franco A, Montalban X, Espejo C. Semaphorins 3A and 7A: potential immune and neuroregenerative targets in multiple sclerosis. *Trends Mol Med* 2013;**19**:157–164.
18. Canto E, Tintore M, Villar LM, Borras E, Alvarez-Cermeno JC, Chiva C, Sabido E, Rovira A, Montalban X, Comabella M. Validation of semaphorin 7A and ala-beta-his-dipeptidase as biomarkers associated with the conversion from clinically isolated syndrome to multiple sclerosis. *J Neuroinflammation* 2014;**11**:181.
19. Hu S, Liu Y, You T, Heath J, Xu L, Zheng X, Wang A, Wang Y, Li F, Yang F, Cao Y, Zhang H, van Gils JM, van Zonneveld AJ, Jo H, Wu Q, Zhang Y, Tang C, Zhu L. Vascular Semaphorin 7A upregulation by disturbed flow promotes atherosclerosis through endothelial beta1 integrin. *Arterioscler Thromb Vasc Biol* 2018;**38**:335–343.
20. Kohler D, Granja T, Volz J, Koeppen M, Langer HF, Hansmann G, Legchenko E, Geisler T, Bakchoul T, Eggstein C, Haberle HA, Nieswandt B, Rosenberger P. Red blood cell-derived semaphorin 7A promotes thrombo-inflammation in myocardial ischemia-reperfusion injury through platelet GPIb. *Nat Commun* 2020;**11**:1315.
21. Hong L, Li F, Tang C, Li L, Sun L, Li X, Zhu L. Semaphorin 7A promotes endothelial to mesenchymal transition through ATF3 mediated TGF-beta2/Smad signaling. *Cell Death Dis* 2020;**11**:695.
22. Thayaparan D, Emoto T, Khan AB, Besla R, Hamidzada H, El-Maklizi M, Sivasubramaniyam T, Vohra S, Hagerman A, Nejat S, Needham-Robbins CE, Wang T, Lindquist M, Botts SR, Schroer SA, Taniguchi M, Inoue T, Yamanaka K, Cui H, Al-Chami E, Zhang H, Althagafi MG, Michalski A, McGrath JJC, Cass SP, Luong D, Suzuki Y, Li A, Abow A, Heo R, Pacheco S, Chen E, Chiu F, Byrne J, Furuyashiki T, Husain M, Libby P, Okada K, Howe KL, Heximer SP, Yamashita T, Wang B, Rubin BB, Cybulsky MI, Roy J, Williams JW, Crome SQ, Epelman S, Hirata KI, Stampfli MR, Robbins CS. Endothelial dysfunction drives atherosclerotic plaque macrophage-dependent abdominal aortic aneurysm formation. *Nat Immunol* 2025;**26**:706–721.
23. Li Z, Zhao Z, Cai Z, Sun Y, Li L, Yao F, Yang L, Zhou Y, Zhu H, Fu Y, Wang L, Fang W, Chen Y, Kong W. Runx2 (runt-related transcription factor 2)-mediated microcalcification Is a novel pathological characteristic and potential mediator of abdominal aortic aneurysm. *Arterioscler Thromb Vasc Biol* 2020;**40**:1352–1369.
24. Meyer RE, Fish RE. A review of tribromoethanol anesthesia for production of genetically engineered mice and rats. *Lab Anim (NY)* 2005;**34**:47–52.
25. Roychowdhury T, Klarin D, Levin MG, Spin JM, Rhee YH, Deng A, Headley CA, Tsao NL, Gellatly C, Zuber V, Shen F, Hornsby WE, Laursen IH, Verma SS, Locke AE, Einarsson G, Thorleifsson G, Graham SE, Dikilitas O, Pattee JW, Judy RL, Pauls-Verges F, Nielsen JB, Wolford BN, Brumpton BM, Dilme J, Peypoch O, Juscafresa LC, Edwards TL, Li D, Banasik K, Brunak S, Jacobsen RL, Garcia-Barrio MT, Zhang J, Rasmussen LM, Lee R, Handa A, Wanhainen A, Mani K, Lindholt JS, Obel LM, Strauss E, Oszkinis G, Nelson CP, Saxby KL, van Herwaarden JA, van der Laan SW, van Setten J, Camacho M, Davis FM, Wasikowski R, Tsoi LC, Gudjonsson JE, Eliason JL, Coleman DM, Henke PK, Ganesh SK, Chen YE, Guan W, Pankow JS, Pankratz N, Pedersen OB, Erikstrup C, Tang W, Hveem K, Gudbjartsson D, Gretarsdottir S, Thorsteinsdottir U, Holm H, Stefansson K, Ferreira MA, Baras A, Kullo IJ, Ritchie MD, Christensen AH, Iversen KK, Eldrup N, Sillesen H, Ostrowski SR, Bundgaard H, Ullum H, Burgess S, Gill D, Gallagher K, Sabater-Lleal M, DiscovEhr, Regeneron Genetics C, Study UKAG, Consortium DG, Program VAMV, Surakka I, Jones GT, Bown MJ, Tsao PS, Willer CJ, Damrauer SM. Genome-wide association meta-analysis identifies risk loci for abdominal aortic aneurysm and highlights PCSK9 as a therapeutic target. *Nat Genet* 2023;**55**:1831–1842.
26. Zheng S, Tsao PS, Pan C. Abdominal aortic aneurysm and cardiometabolic traits share strong genetic susceptibility to lipid metabolism and inflammation. *Nat Commun* 2024;**15**:5652.
27. Woo SH, Kyung D, Lee SH, Park KS, Kim M, Kim K, Kwon HJ, Won YS, Choi I, Park YJ, Go DM, Oh JS, Yoon WK, Paik SS, Kim JH, Kim YH, Choi JH, Kim DY. TXNIP suppresses the osteochondrogenic switch of vascular smooth muscle cells in atherosclerosis. *Circ Res* 2023;**132**:52–71.
28. Willems BA, Furmanik M, Caron MMJ, Chatrou MLL, Kusters DHM, Welting TJM, Stock M, Rafael MS, Viegas CSB, Simes DC, Vermeer C, Reutelingsperger CPM, Schurgers LJ. Ucma/GRP inhibits phosphate-induced vascular smooth muscle cell calcification via SMAD-dependent BMP signalling. *Sci Rep* 2018;**8**:4961.
29. Zhao Y, Huang Z, Gao L, Ma H, Chang R. Osteopontin/SPP1: a potential mediator between immune cells and vascular calcification. *Front Immunol* 2024;**15**:1395596.
30. Bersini S, Schulte R, Huang L, Tsai H, Hetzer MW. Direct reprogramming of human smooth muscle and vascular endothelial cells reveals defects associated with aging and Hutchinson-Gilford progeria syndrome. *Elife* 2020;**9**:e54383.
31. Goncalves I, Oduor L, Matthes F, Rakem N, Meryn J, Skenteris NT, Aspberg A, Orho-Melander M, Nilsson J, Matic L, Edsfeldt A, Sun J, Bengtsson E. Osteomodulin gene expression is associated with plaque calcification, stability, and fewer cardiovascular events in the CPIP cohort. *Stroke* 2022;**53**:e79–e84.
32. Guo M, Ji S, Wang H, Zhang J, Zhu J, Yang G, Chen L. Myeloid cell mPGES-1 deletion attenuates calcium phosphate-induced abdominal aortic aneurysm in male mice. *Inflammation* 2025;**48**:288–298.
33. Tian K, Malik F, Zhao S. Animal models for abdominal aortic aneurysms: where we are and where we need to go. *Animal Model Exp Med* 2025;**8**:573–577.
34. Tovell H, Testa A, Zhou H, Shpiro N, Crafter C, Ciulli A, Alessi DR. Design and characterization of SGK3-PROTAC1, an isoform specific SGK3 kinase PROTAC degrader. *ACS Chem Biol* 2019;**14**:2024–2034.
35. Li F, Yi Y, Miao Y, Long W, Long T, Chen S, Cheng W, Zou C, Zheng Y, Wu X, Ding J, Zhu K, Chen D, Xu Q, Wang J, Liu Q, Zhi F, Ren J, Cao Q, Zhao W. N(6)-methyladenosine modulates nonsense-mediated mRNA decay in human glioblastoma. *Cancer Res* 2019;**79**:5785–5798.
36. Yuan S, Xi S, Weng H, Guo MM, Zhang JH, Yu ZP, Zhang H, Yu Z, Xing Z, Liu MY, Ming DJ, Sah RK, Zhou Y, Li G, Zeng T, Hong X, Li Y, Zeng XT, Hu H. YTHDC1 as a tumor progression suppressor through modulating FSP1-dependent ferroptosis suppression in lung cancer. *Cell Death Differ* 2023;**30**:2477–2490.
37. Tamagnone L, Artigiani S, Chen H, He Z, Ming GI, Song H, Chedotal A, Winberg ML, Goodman CS, Poo M, Tessier-Lavigne M, Comoglio PM. Plexins are a large family of receptors for transmembrane, secreted, and GPI-anchored semaphorins in vertebrates. *Cell* 1999;**99**:71–80.
38. Hu P, Miller AE, Yeh CR, Bingham GC, Civelek M, Barker TH. SEMA7a primes integrin alpha5beta1 engagement instructing fibroblast mechanotransduction, phenotype and transcriptional programming. *Matrix Biol* 2023;**121**:179–193.

39. Korner A, Kohler D, Schneider M, Roth JM, Granja TF, Eggstein C, Mirakaj V, Rosenberger P. Semaphorin 7A is protective during inflammatory peritonitis through integrin receptor signaling. *Front Immunol* 2023;**14**:1251026.
40. Wu X, Meng Y, Wang C, Yue Y, Dong C, Xiong S. Semaphorin7A aggravates coxsackievirusB3-induced viral myocarditis by increasing alpha1beta1-integrin macrophages and subsequent enhanced inflammatory response. *J Mol Cell Cardiol* 2018;**114**:48–57.
41. Huang J, Zhao C, Zhang S. Semaphorin 7A promotes endothelial permeability and inflammation via plexin C1 and integrin beta1 in Kawasaki disease. *BMC Pediatr* 2024;**24**:285.
42. Tang Z, Xie J, Jin M, Wei G, Fu Z, Luo X, Li C, Jia X, Zheng H, Zhong L, Li X, Wang J, Chen G, Chen Y, Liao W, Liao Y, Bin J, Huang S. Sympathetic hyperinnervation drives abdominal aortic aneurysm development by promoting vascular smooth muscle cell phenotypic switching. *J Adv Res* 2025;**71**:383–398.
43. Wang Y, Dong CQ, Peng GY, Huang HY, Yu YS, Ji ZC, Shen ZY. MicroRNA-134-5p regulates Media degeneration through inhibiting VSMC phenotypic switch and migration in thoracic aortic dissection. *Mol Ther Nucleic Acids* 2019;**16**:284–294.
44. Basnet R, Gong GQ, Li C, Wang MW. Serum and glucocorticoid inducible protein kinases (SGKs): a potential target for cancer intervention. *Acta Pharm Sin B* 2018;**8**: 767–771.
45. Liu J, Chai XX, Qiu XR, Sun WJ, Tian YL, Guo WH, Yin DC, Zhang CY. Type X collagen knockdown inactivate ITGB1/PI3 K/AKT to suppress chronic unpredictable mild stress-stimulated triple-negative breast cancer progression. *Int J Biol Macromol* 2024;**273**:133074.
46. Yang L, Zhu J, Yang L, Gan Y, Hu D, Zhao J, Zhao Y. SCO-spondin-derived peptide NX210 rescues neurons from cerebral ischemia/reperfusion injury through modulating the Integrin-beta1 mediated PI3 K/Akt pathway. *Int Immunopharmacol* 2022;**111**:109079.
47. Yan L, Zhou R, Feng Y, Li R, Zhang L, Pan Y, Qiao X, Li P, Wei X, Xu C, Li Y, Niu X, Sun X, Lv Z, Tian Z. MiR-134-5p inhibits the malignant phenotypes of osteosarcoma via ITGB1/MMP2/PI3 K/Akt pathway. *Cell Death Discov* 2024;**10**:193.
48. Chen M, Yang D, Zhou Y, Yang C, Lin W, Li J, Liu J, Ye J, Huang W, Ma W, Li W, Chen J, Zhang Y, Shi GP, Luo J, Li J, Luo S. Colchicine blocks abdominal aortic aneurysm development by maintaining vascular smooth muscle cell homeostasis. *Int J Biol Sci* 2024;**20**:2092–2110.
49. Wang Q, Zhou T, Liu Z, Ren J, Phan N, Gupta K, Stewart DM, Morgan S, Assa C, Kent KC, Liu B. Inhibition of receptor-interacting protein kinase 1 with necrostatin-1 s ameliorates disease progression in elastase-induced mouse abdominal aortic aneurysm model. *Sci Rep* 2017;**7**:42159.
50. You T, Zhu Z, Zheng X, Zeng N, Hu S, Liu Y, Ren L, Lu Q, Tang C, Ruan C, Zhang Y, Zhu L. Serum semaphorin 7A is associated with the risk of acute atherothrombotic stroke. *J Cell Mol Med* 2019;**23**:2901–2906.